1 July 2001

ELSEVIER

Optics Communications 194 (2001) 109–129

OPTICS COMMUNICATIONS

www.elsevier.com/locate/optcom

Extraction of laser rate equations parameters for representative simulations of metropolitan-area transmission systems and networks

Ioannis Tomkos *, Ioannis Roudas, Robert Hesse, Neophytos Antoniades, Aleksandra Boskovic, Richard Vodhanel

Corning Inc., Photonics Research and Test Center, 2200 Cottontail Lane, Somerset, NJ 08873, USA

Received 15 January 2001; received in revised form 30 March 2001; accepted 4 April 2001

Abstract

In this paper we present procedures for the extraction of laser rate equation parameters. The parameters are extracted using fitting of static and dynamic measurements with simple theoretical expressions. In particular, chirp related parameters are extracted directly through measured chirp and power waveforms. The extracted parameters are used in a large-signal rate equation laser model to calculate the power and chirp waveforms. The simulations are compared with experiments and the agreement is excellent. The procedures have been applied to directly modulated lasers having different chirp characteristics and designed for either 2.5 or 10 Gb/s operation. Using the rate equation laser model with the extracted parameters, we performed a simulation study to identify the value of employing a negative dispersion fiber in metro-area networks. It is shown that dispersion shifted fibers with negative dispersion across the entire usable fiber bandwidth (1280–1620 nm) advances the performance of directly modulated lasers used in wavelength division multiplexed metropolitan-area transmission systems and networks. At 2.5 Gb/s transmission over 300 km of negative dispersion fibers is possible for directly modulated lasers across the erbium doped fiber amplifier bandwidth, while at 10 Gb/s an impressive distance of 100 km can be achieved.

1. Introduction

The characteristics of the cost-sensitive metropolitan-area networks, in terms of transmission distance and bit rate, are not so demanding compared to long-haul networks and therefore the requirements on the performance of the optical devices are somewhat relaxed. Therefore, cost-effective directly modulated lasers (DML) have attracted recently much attention for metro-area applications. However, DMLs have some drawbacks [1]. The interaction of the laser chirp with the dispersion of conventional single-mode fibers deteriorates the signal and limits the maximum transmission distance [1–3]. In metro-area networks utilizing DMLs, this chirp-induced distortion is the major impairment. Therefore, the most critical requirement from a DML is the low dispersion penalty. The use of negative dispersion

* Corresponding author. Tel.: +1-732-748-3744; fax: +1-732-748-3760.

E-mail address: tomkosi@corning.com (I. Tomkos).

0030-4018/01/$ - see front matter
PII: S0030-4018(01)01230-5

fibers to enhance the transmission distances of DML has been discussed recently [4,5].

Computer simulations are useful in order to predict the system behavior at the design stage. For example, the choice of transmission fiber characteristics for optimum performance in metro-area networks should first be determined through simulations that will identify the transmission performance of DMLs. The model that a designer should select and the simulation parameters involved in it should be sufficiently accurate in order to obtain useful conclusions on the design and performance of the real system. For example, the identification of the parameters of an optical fiber that will enhance the transmission performance of DML should be performed through a simulation study. Many laser models exist in the literature with various degrees of complexity, each having its own advantages and disadvantages [6–14]. For the purpose of evaluation of the dispersion penalty, the use of the laser rate equations has been favored in the literature [6–10,14]. These equations describe the time evolution of the carrier density (N), the photon density (S) and the phase (ϕ). It has been acknowledged that using the rate equations the laser dynamics can be evaluated sufficiently accurate. A large variety of rate equation based models have been published in the literature having different degrees of complexity [6–10,14]. The complex models provide an in-depth insight into the laser properties, but require a large number of parameters to be either assumed or measured. However, for system simulation purposes a simple model is adequate. The number of parameters that have to be known or determined should be reduced to a minimum value, in order to have representative simulation results that have a very good agreement with the experiment. Therefore, in this study we use the well-known large signal single mode laser rate equations in their simpler form [6]: [1]

$$\frac{dS(t)}{dt} = \frac{\Gamma g_0(N(t)-N_0)}{1+\varepsilon S(t)} S(t) - \frac{S(t)}{\tau_p} + \frac{\Gamma \beta N(t)}{\tau_c} \quad (1)$$

$$\frac{dN(t)}{dt} = \frac{I(t)}{eV} - \frac{N(t)}{\tau_c} - \frac{g_0(N(t)-N_0)}{1+\varepsilon S(t)} S(t) \quad (2)$$

$$\frac{d\phi}{dt} = \frac{\alpha}{2}\left[\Gamma g_0(N(t)-N_0) - \frac{1}{\tau_p}\right] \quad (3)$$

The output power $P(t)$ is related to the photon density $S(t)$ through the relation:

$$P(t) = \frac{V\eta h v}{2\Gamma\tau_p} S(t) \quad (4)$$

In the above equations, [2] $I(t)$ is the current waveform injected in the active layer, $S(t)$ is the photon density, $N(t)$ is the carrier density, v is the optical frequency, h is the Planck's constant, η is the differential quantum efficiency, Γ is the confinement factor, N_0 is the carrier density at transparency, β is the fraction of spontaneous emission noise coupled into the lasing mode, g_0 is the differential gain coefficient, ε is the nonlinear gain compression factor (gain saturation coefficient), τ_p is the photon lifetime, τ_c is the carrier lifetime, V is the volume of the active layer and α is the line width enhancement factor. It should be noticed that the parameters appearing in these equations should be treated as effective parameters that accompany the specific model, which are somewhat detached from their physical origin. Also, static temperature dependence of the value of each parameter is difficult to be implemented. The effect of temperature dependence of the parameter values could be taken into account by unifying the temperature dependence of all parameters in a temperature-dependent injection efficiency as in Ref. [9], but this approach, in a first approximation, has been ignored in the contents of the present study.

In Eqs. (1)–(4) the minimum number of parameters that have to be estimated is ten

[1] It should be noted that Eqs. (1)–(3) could also be used for modeling the dynamic behavior of a directly modulated DFB laser, although the exact structure of the DFB laser is not taken into account. The coupling strength of the grating in the DFB laser is effectively taken into account in the value of the photon lifetime.

[2] This set of laser rate equations can be solved numerically using for example an adaptive step-size fifth order Runge–Kutta method [15].

(Γ, V, N_0, β, g_0, ε, τ_p, τ_c, η and α), in addition to the lasing wavelength λ. Their values vary from one laser diode to another and different sets of parameters may appear very detrimental for the low dispersion penalty performance of the laser transmitter. The information given in data sheets by the laser manufacturers is insufficient for the extraction of the parameters. To our knowledge, it is not possible to determine experimentally with a single measurement each one of the actual rate equation parameters from a packaged device [16]. However, it is possible to determine through measurements, certain combinations of the parameters and a limited set of the actual rate equation parameters [17]. Therefore, it is of great interest to establish simple and accurate parameter extraction procedures through measurements on a packaged device.

Many works have been published during the recent years dealing with the extraction of the rate equation parameters [17–19]. We will review the results presented in the previous works. Cartledge and Srinivasan [18] have used a parameter extraction procedure based on: (a) measurements of the threshold current, the output power, the resonance frequency and the damping factor and (b) fitting the measured results with the simulation results calculated using the rate equations for various sets of the rate equation parameters. However, their procedure resulted in a number of different sets of the actual rate equation parameters that could fit the experimental results. The robustness of their procedure had been tested mainly through comparison of (a) the simulated results with measurements of the chirp waveform of a certain DFB laser and (b) the dependence of the receiver sensitivity on the amplitude of the modulation current. It should be noted that the chirp waveform depends primarily on the value of the α-parameter, which was not measured or calculated. No parameter related with the laser parasitics was extracted. The comparisons that were made showed good agreement between theory and experiment. Bjerkan et al. [17] have presented procedures in which they extracted combinations of parameters directly through certain static and small signal RF measurements. Part of the procedures was the measurement of the FM characteristics using three different methods. In this way, they were able to extract parameters directly related with the chirp characteristics, the α-parameter and the ratio ε/g_0. Their procedure was tested through comparison of the measured and simulated amplitude waveforms before and after transmission over standard single mode fiber. For some cases the comparison was fairly good. No comparison of the chirp waveforms was reported. No parameter related with the laser parasitics was extracted. Czotscher et al. [19] have developed a DML model which is based on a more complicated set of rate equations with a larger number of parameters. They also used static and small signal RF measurements for the determination of some of the rate equation parameters and also of the cut-off frequency of the parasitics transfer function. In order to validate their model and the parameter extraction procedures used comparisons of the measured and simulated results for both chirp and intensity waveforms were performed. The simulations were in very good agreement with the experiment. However, their model required knowledge of some parameters, which cannot be determined through measurements on a packaged device. All the aforementioned efforts have offered very important contributions for the extraction of rate equations parameters from a packaged device and to the understanding of the dependence of the characteristics of the output field of the DMLs on the parameter values. However, no single work offers a complete and accurate characterization using parameters that all have extracted through measurements.

This paper will present a detailed study on the extraction procedures of laser rate equation parameters. Some of the procedures have been already published in the literature in various papers, while some others are presented here for the first time. The specific parameter extraction procedures that will be presented here will result in parameter values, which will be used in the model and will simulate the laser dynamics in an accurate way. Comparisons of the measured and simulated results for both chirp and intensity waveforms will be used to present the validity of the model used and of the parameter extraction procedures followed. The extraction procedures have been

applied for the characterization of five DMLs from different vendors. The agreement between the measured and simulated results is exceptional. The extracted parameters were then used in transmission simulations to identify the best fiber choice for metro-area networks utilizing DMLs. Fibers with different amounts and signs of dispersion were tested. This work can be a useful tool whenever the influence of DML characteristics on the overall performance of a system must be accurately evaluated.

2. Theoretical background for the parameter extraction procedures

2.1. Steady state measurements – power versus bias current

A first set of parameters can be extracted from measurements of the optical power at the output of the DML versus the bias current [17]. Following Ref. [17], and assuming that $\varepsilon/g_0\tau_c \ll 1$, $\beta \ll 1$, the expression that determines analytically the P–I curve can be derived:

$$\Phi^2P^2 - \Phi[I - I_{th} - I_S]P - I_SI = 0 \tag{5}$$

where:

$$\Phi = \frac{2e\lambda}{hc\eta} \tag{6}$$

$$I_{th} = \frac{eV}{\tau_c}\left(N_0 + \frac{1}{\Gamma g_0\tau_p}\right) \tag{7}$$

$$I_S = \frac{\beta eV}{\Gamma g_0\tau_c\tau_p} \tag{8}$$

By numerical fitting of the experimentally obtained P–I curve to the positive solution of Eq. (5), the quantity Φ (or equivalently the quantum efficiency η), the threshold current I_{th}, and the quantity I_S, can be determined. Alternatively, the threshold current and the slope can be calculated from measurements above threshold and these values could be used in Eq. (5) for the determination of the parameter I_S.

2.2. Dynamic measurements – IM frequency response measurements

Measurements of the resonance frequency and the damping factor for various bias currents could provide a significant insight to the laser dynamics [17–21]. The measurements can also be used for the determination of intrinsic device parameters such as the differential gain g_0, the carrier lifetime τ_c and the nonlinear gain compression factor ε, which are critical for the dynamic behavior of a laser diode [17–19]. In order to extract the values of the resonance frequency and the damping factor, measurements of the small signal IM frequency response of the laser are needed [17–21]. By applying small signal intensity modulation to the laser diode we could extract its intrinsic small signal IM frequency response. Numerical fitting of the experimentally obtained IM response with the known theoretical expression of the small signal IM response of the laser [18,21], will determine the resonance frequency and the damping factor. It should be noted that although the measurements are performed for the small signal regime, the extracted parameters could be used in the large signal calculations based on the rate equation model.

The expression we used for the small signal IM frequency response $H(f)$ of a laser diode is [19]:

$$H(f) = \frac{Z}{(i2\pi f)^2 + i2\pi f\Gamma_d + Z} \tag{9}$$

where f is the modulation frequency, Γ_d is the damping factor, and Z is a parameter related to the damping factor and the resonance frequency. The resonance frequency (f_r) is related to Z and Γ_d through the expression:

$$f_r = \frac{1}{2\pi}\sqrt{Z - \frac{1}{2}(\Gamma_d)^2} \tag{10}$$

where it can be shown that:

$$Z = \frac{\Gamma g_0}{eV}(I_{bias} - I_{th}) - \left(\frac{\Gamma}{eV}\right)^2 \varepsilon g_0\tau_p(I_{bias} - I_{th})^2 \tag{11}$$

$$\Gamma_d = \frac{1}{\tau_c} + \frac{\Gamma g_0}{eV}\left(\tau_p + \frac{\varepsilon}{g_0}\right)(I_{bias} - I_{th}) - \left(\frac{\Gamma}{eV}\right)^2 \varepsilon g_0 \tau_p \left(\tau_p + \frac{\varepsilon}{g_0}\right)(I_{bias} - I_{th})^2 \quad (12)$$

If we make the assumption that $(\Gamma_d)^2 \ll 2Z$ (which is valid for small bias currents), then $Z = (2\pi f_r)^2$ and the following expression hold [17,19]:

$$f_r = \sqrt{\frac{\Gamma g_0}{4\pi^2 eV}(I_{bias} - I_{th})} \quad (13)$$

The damping frequency is related to the resonance frequency through the expression:

$$\Gamma_d = \frac{1}{\tau_c} + K f_r^2 \quad (14)$$

where:

$$K = 4\pi^2\left(\tau_p + \frac{\varepsilon}{g_0}\right) \quad (15)$$

As pointed out in Ref. [18], in several previous studies related with the extraction of the resonance frequency and the damping factor [17,19,20] instead of Eq. (11) a more simplified equation for the small signal IM response has been used:

$$H(f) = \frac{f_r^2}{(f_r^2 - f_r^2) + i2\Gamma_d f/2\pi} \quad (16)$$

Eq. (18) results from Eq. (11) if the approximation:

$$f_r = \frac{1}{2\pi}\sqrt{Z} \quad (17)$$

is valid. However, Eq. (19) is valid only for small bias currents. The use of Eq. (9) instead Eq. (16) will increase the accuracy of the results [18]. Therefore, in the following we used Eq. (9) together with the more accurate expressions (11) and (12) in order to do the fittings.

By repeating the fitting procedure for curves corresponding to different bias current levels and plotting the values of the parameters f_r, Γ_d as a function of the bias current, the parameter τ_c, the universal K-factor, and the quantity $\Gamma g_0/V$ can be calculated.

2.3. Dynamic measurements – measurements of dynamic waveforms

2.3.1. Intensity waveform

The measured intensity waveform will yield insight about the dynamic laser behavior. Features such as the "ringing" on the 1's and the 0's, the power overshoot on the 1's, and the rise and fall time of the optical pulse are of interest for the understanding of the performance of the DMLs. Furthermore, the power waveform ($P(t)$) is needed for the calculation of the chirp waveform ($\Delta v(t)$).

2.3.2. Chirp waveform

An important effect arising from the nonlinearity of the laser is that the output optical frequency varies in response to variations in the drive current, a property known as frequency chirp [1–8,22–25]. It is well known that the chirp greatly affects the pulse propagation, causing the leading and trailing edges of the pulses to have slightly different frequencies and consequently different group velocities.

At this point we should mentioned that in the previous parameter extraction studies [17,19] the chirp waveforms were either not measured or not used for extraction of chirp related parameters. The α-parameter, where extracted and not assumed, has been determined using the method presented in Ref. [26].

Here, we measured the chirp waveform using a technique similar to Ref. [27] and we have extracted useful parameters from these measurements. The procedure is as follows: once the intensity waveform is known, the measured chirp waveform can be used in order to be fitted with the theoretical expression that relates the chirp with the laser output optical power [2]:

$$\Delta v(t) = \frac{\alpha}{4\pi}\left(\frac{d}{dt}[\ln(P(t))] + \kappa P(t)\right) \quad (18)$$

From this procedure, the α-parameter can be calculated as well as the adiabatic chirp coefficient κ, which is directly related to the nonlinear gain compression factor:

$$\kappa = \frac{2\Gamma}{\eta h v V}\varepsilon \quad (19)$$

In expression (18), the first term is a structure-independent "transient" chirp and the second term is a structure-dependent "adiabatic" chirp [8]. The first term has a significant value during relaxation oscillations. The second term is related to the relaxation oscillation damping since, as can be seen from Eq. (1), is directly proportional to the gain compression factor. It is worth pointing out that the selected value of ε at the laser design stage will be a tradeoff between the amount of transient and adiabatic chirp, while will determine, to some extent, the useful modulation bandwidth. Dynamic thermal effects (thermal chirp) which affect only long sequences of 1's and 0's, could be ignored in a first approximation if the bit rate of interest is larger than 2.5 Gb/s.

3. Experimental procedures for the measurements needed

3.1. Steady state measurements

(a) Wavelength: The lasing wavelength λ (or equivalently the optical frequency v) is measured using an optical spectrum analyzer or a wavemeter.

(b) Power versus current curve: To measure the *P–I* curve the laser is set to operate in continuous wave mode. Well above threshold, the power versus current characteristics are measured by changing the bias current of the laser driver and measuring the output optical power using either an optical powermeter or an optical spectrum analyzer. Near and below threshold the optical spectrum analyzer in high sensitivity mode should be used for the power measurements. In this way we can avoid fault measurements due to the presence of side modes.

3.2. Dynamic measurements – IM frequency response measurements

The small signal AM response can be measured using a lightwave component analyzer. The current of the laser diode is directly modulated by an RF signal. The frequency of the RF signal is swept in all the available bandwidth of the analyzer. The corresponding trace is recorded and the procedure is repeated for several bias currents. Unfortunately, the recorded traces correspond to the combined effect of: (a) the internal laser IM response, (b) the effect of the parasitics and (c) any artifacts produced by the lightwave component analyzer. In order to avoid any artifact of the measuring equipment and the effect of the parasitics that will have an impact in the fitting procedure, the procedure described in Ref. [20] should be applied. The IM response curve (in dB) corresponding to a bias current close to threshold is subtracted from all the other curves. The resulting experimental curves should be fitted using the expression [18]:

$$H(f) = \left[\mathrm{Abs}\left(\frac{Z}{(\mathrm{i}2\pi f)^2 + \mathrm{i}2\pi f \Gamma_\mathrm{d} + Z}\right)_{I_\mathrm{bias}}\right]_\mathrm{dB} - \left[\mathrm{Abs}\left(\frac{Z}{(\mathrm{i}2\pi f)^2 + \mathrm{i}2\pi f \Gamma_\mathrm{d} + Z}\right)_{I_\mathrm{th}}\right]_\mathrm{dB} \tag{20}$$

The important property of this technique is that it almost eliminates any limitations that could arise from the mounting fixture and the packaging of the laser, in addition to relaxing the requirements for accurate calibration of the experimental setup.

3.3. Dynamic measurements – measurements of dynamic waveforms

The intensity waveform is recorded using a communications analyzer. The recordings are made for several average output powers and extinction ratios. The chirp waveform is recorded using a chirp measurement equipment [3] and a communications analyzer. The recordings are made for several average output powers and extinction ratios. The measurement can be performed with lasers having arbitrary chirp characteristics.

[3] This equipment is essentially an interferometer [28]. For details about the operation principle see Refs. [27,28].

Table 1
Specified characteristics by the vendors for each one of the DMLs under characterization

	Wavelength (nm)	Threshold current (mA)	Line width at −20 dB (nm)	Side mode suppression ratio (dB)
2.5 Gb/s DML-1	1554.62	4.7	0.25	44.2
2.5 Gb/s DML-2	1544.51	16.31	0.40	40
10 Gb/s DML	1541.35	15.5	0.45	42

4. How can we use the extracted parameters

From all the above procedures the parameters: η, I_{th}, I_S, τ_c, K, Γg_0, α, κ can be directly extracted from the measurements. Using these parameters one should calculate the actual rate equation parameters if the laser model described by Eqs. (1)–(4) is to be used. Assuming a certain value for the volume of the active region (V), and using the values of η and κ, the quantity $\Gamma\varepsilon$ can be calculated from Eq. (19). From this value and the value of Γg_0, the quantity ε/g_0 is known. Then, using this value in Eq. (15) the parameter τ_p can be calculated. Using the values of V, Γg_0, τ_p and τ_c, the parameter β can be calculated from Eq. (8). Also, using the values of V, Γg_0, τ_p and τ_c in Eq. (7), the parameter N_0 can be calculated. Finally, assuming a specific value for Γ the parameters g_0 and ε can be calculated. The assumed Γ and V are in fact dummy parameters and their selection will not affect the results for the calculation of the output field from the DMLs.

Alternatively, we can modify the rate equations to only have the measured parameters appearing in the new set. The modified set of rate equations that can be used for the simulations is reported in Ref. [17].

5. Results and discussion

5.1. Characteristics of the DMLs under test

Various DMLs from different vendors were fully characterized and parameters were extracted for each one of them. In the following we will present the results of our parameter extraction procedures for two 2.5 Gb/s and one 10 Gb/s commercially available DMLs. Results for 10 Gb/s DMLs are reported for the first time to our knowledge. The 2.5 Gb/s DML were rated for less that 2 dB chirp induced power penalty for a dispersion/distance product of 1800 ps/nm and for a dynamic extinction ratio larger than 8.2 dB. The 10 Gb/s DML was rated for 10 km-transmission distance over SMF-28 fiber with a bit error rate of 10^{-10} for a dynamic extinction ratio of 8.2 dB. The specified characteristics from the vendors for each one of the DMLs are listed in Table 1.

In Fig. 1 the measured transmitter eye patterns for the three DMLs are shown. For the 2.5 Gb/s DMLs the dynamic extinction ratio was 8.2 dB and the average optical power 1 mW, while for the 10 Gb/s DML the dynamic extinction ratio was 8.2 dB and the average optical power 4.46 mW. The eye diagrams for the 2.5 Gb/s DMLs were obtained without using an electrical filter after the receiver. The 2.5 Gb/s DML-1 does not present any ringing either on the top or the bottom of the eye. However, it has a significant large rise and fall time that result in a reduced eye height. The 2.5 Gb/s DML-2 presents a significant ringing on the top of the eye. The fall time is considerably larger than the rise time. The 10 Gb/s DML presents an extremely large ringing on both the top and the bottom of the eye. Therefore, the eye diagram in this case was measured using an electrical filter after the receiver. The eye is asymmetric with a larger fall time compared to the rise time.

5.2. Steady state measurements – power versus current curve

In Fig. 2 the measured P–I curve for each DML is shown. The three DMLs under study exhibiting different threshold currents and different efficiencies (different slopes). In Fig. 3 the measured power versus bias current curve is shown together

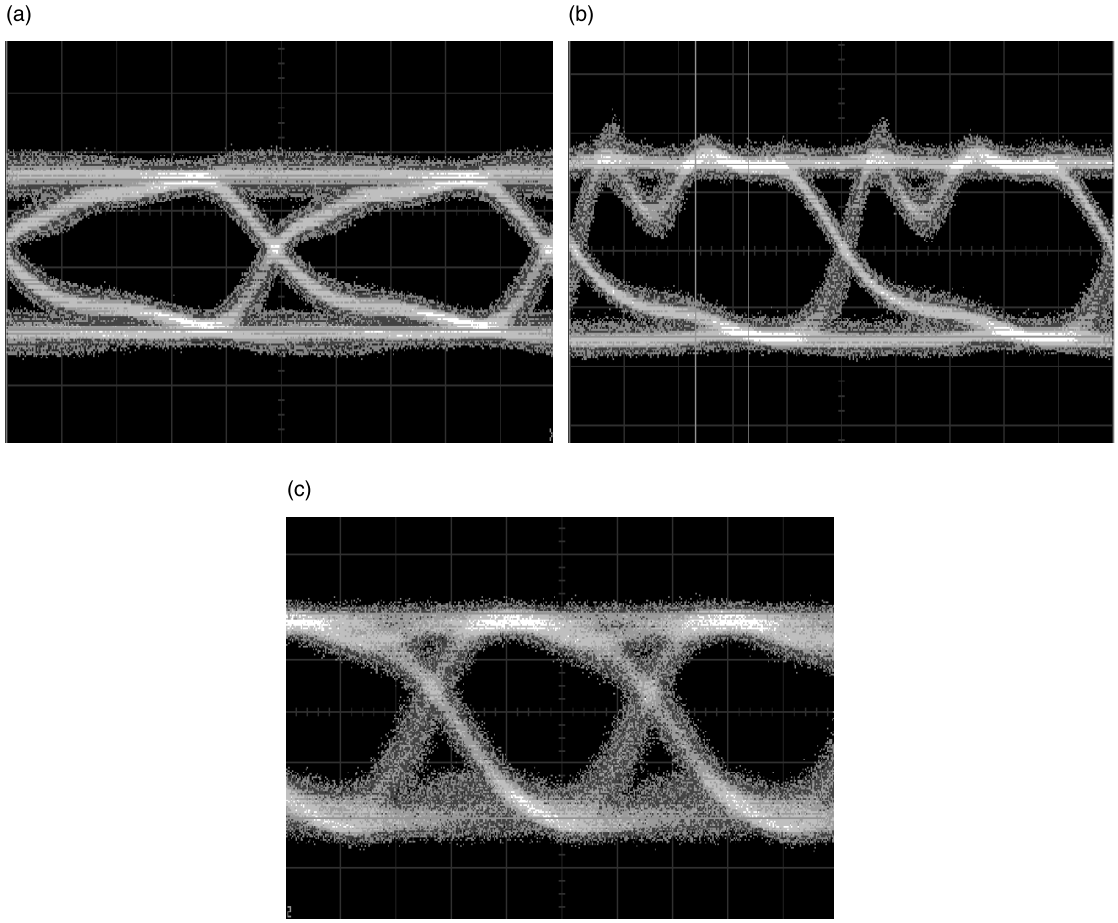

Fig. 1. Eye patterns for (a) 2.5 Gb/s DML-1, (b) 2.5 Gb/s DML-2, (c) 10 Gb/s DML.

with the fitted curve using Eq. (5) for each DML. The fitting is considerably very good, except for the region that corresponds to below threshold operation. The parameters resulting from the fitting of the curves are listed in Table 2. The value of I_S suffered from the largest uncertainty, since it is a parameter related with the portion of the curve that is below threshold.

5.3. Dynamic measurements – power and chirp waveforms

In Fig. 4 the power and chirp waveforms, measured with the chirp measurement equipment, are shown. This time-resolved chirp measurement for the extraction of the α-parameter is similar to what used in Ref. [29]. However, in Ref. [29] the authors used the time-resolved chirp measurements for the characterization of an external modulator that present only transient chirp. The expression used for the extraction of the α-parameter is therefore accurate. However, if the same expression is applied to a DML that presents also adiabatic chirp the extraction of the α-parameter will not be accurate.

The 2.5 Gb/s DML-1 (Fig. 4(a)) is clearly adiabatic chirp dominated as can be seen from the chirp waveform. The transient chirp has been completed masked by the adiabatic chirp component. The peak-to-peak chirp is approximately 7 GHz, a relatively small value. These characteristics imply that the α-parameter and the adiabatic chirp

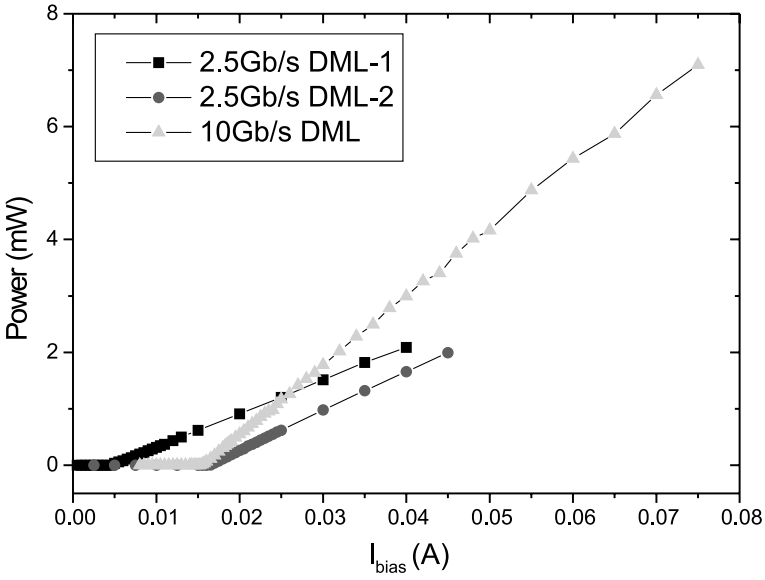

Fig. 2. Power versus current characteristics for the three DMLs.

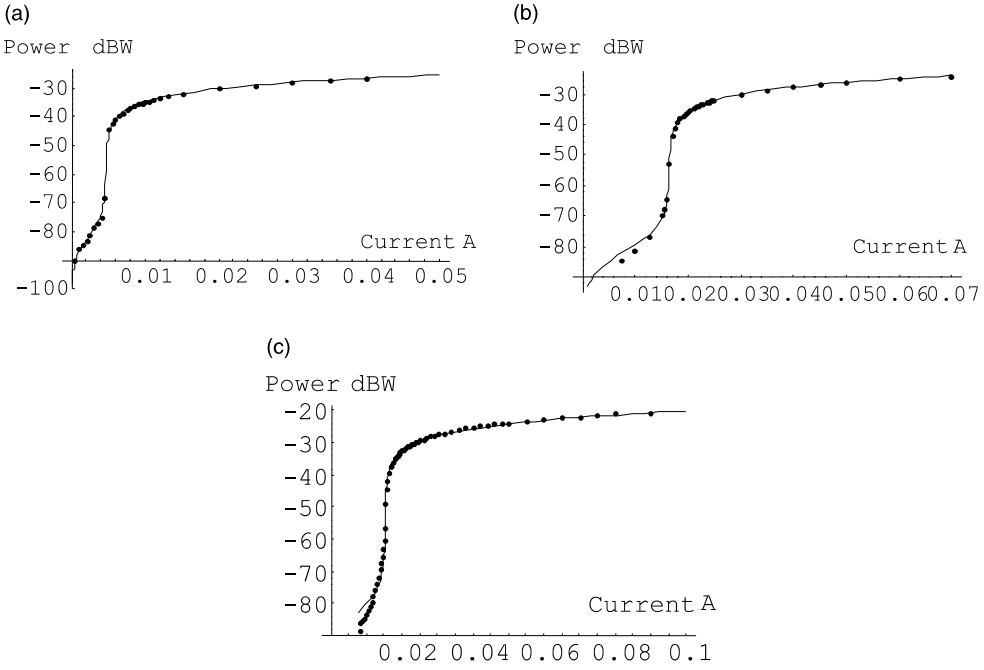

Fig. 3. Power (in log-scale) versus current curve for (a) 2.5 Gb/s DML-1, (b) 2.5 Gb/s DML-2, (c) 10 Gb/s DML. The lines are the fitted curves.

coefficient (κ) have small values. The power waveform shows a small power overshoot on both 1's and 0's. A very good damping of the relaxation oscillations on the 1's and the 0's is also evident.

Table 2
Extracted parameters from the power versus current measurements for each DML

Parameter	Units	2.5 Gb/s DML-1	2.5 Gb/s DML-2	10 Gb/s DML
Φ	A/W	16.35	14.48	8.91
I_{th}	mA	4.66	17.34	15.25
I_S	A	11.2×10^{-8}	7.3×10^{-8}	4.3×10^{-8}

We should notice a rather unusual behavior of the 2.5 Gb/s DML-1. In isolated 1's a power overshoot appears at the trailing edge of the pulse and not at the leading edge as it is the usual case. This behavior is attributed to the characteristics of the parasitics for this DML at it will be shown later on.

The 2.5 Gb/s DML-2 (Fig. 4(b)) is transient chirp dominated. The adiabatic chirp component is significantly lower than the transient chirp component. The peak-to-peak chirp is approximately 30 GHz, a value that results in considerably broad spectrum and consequently increased dispersion penalty for transmission over positive dispersion fibers. These characteristics imply that the α-parameter has a large value while the adiabatic chirp coefficient (κ) has a small value. The power waveform shows a large power overshoot on the 1's while the overshoot on the 0's is small. The damping of the relaxation oscillations on both the 1's and the 0's is not fast. In the case of small power levels the measurements provided by the chirp measurement equipment are not so accurate.

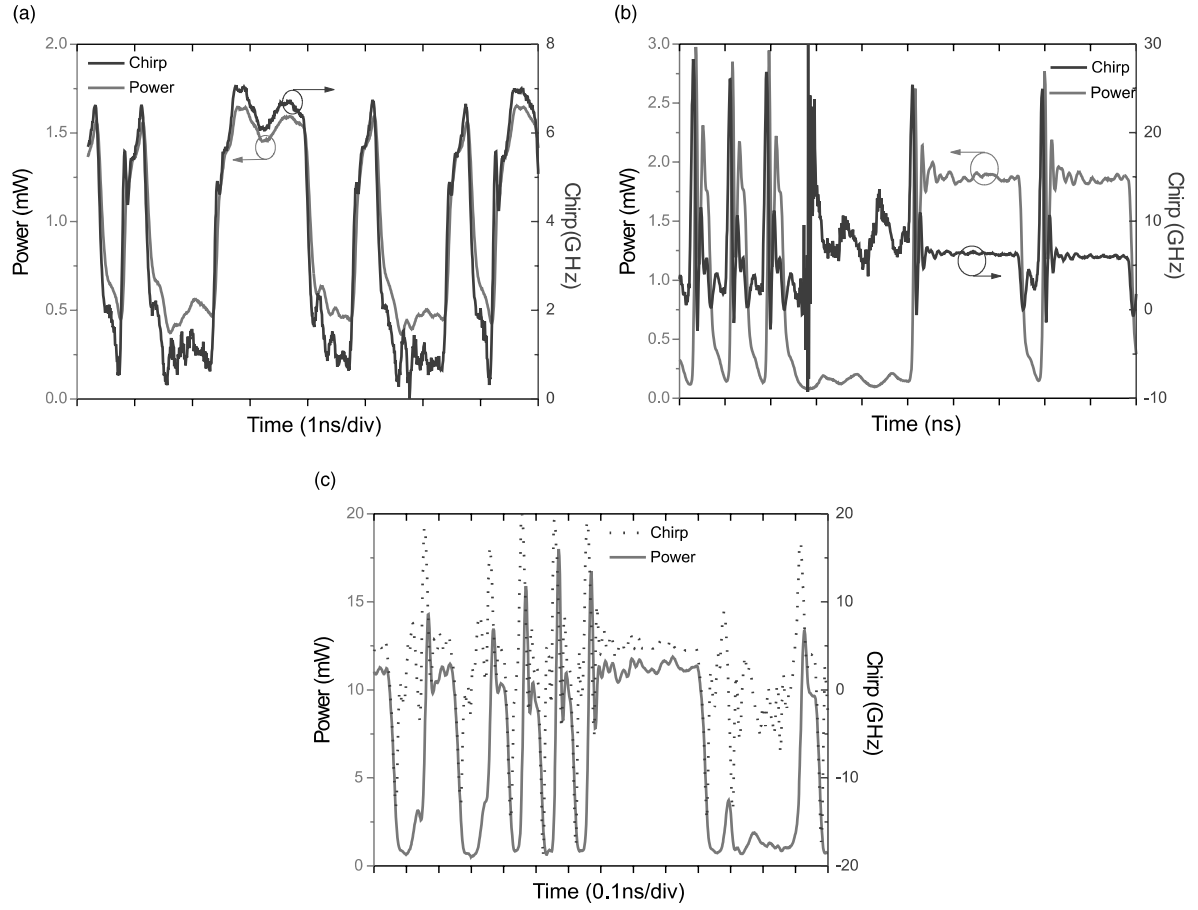

Fig. 4. Power and chirp waveforms for (a) 2.5 Gb/s DML-1, (b) 2.5 Gb/s DML-2, (c) 10 Gb/s DML.

That's the reason why the chirp in Fig. 4(b) appears to be very large during consecutive 1's.

The 10 Gb/s DML (Fig. 4(c)) is also transient chirp dominated. The peak-to-peak chirp is approximately 25 GHz. The power waveform shows a large power overshoot on the 1's and very small undershoot on the 0's. The damping of the relaxation oscillations on both the 1's and the 0's is not fast.

In Fig. 5 the measured chirp waveform is shown together with the fitted curve, using Eq. (18), for each DML. The fitting is exceptional, except for the regions that correspond to low power levels (0's). For such low power levels the chirp measurements are not accurate, which explains, to some extent, the discrepancies between the fitted simulation results and the measurements. The parameters resulting from the fitting of these curves are listed in Table 3. The value of the adiabatic chirp coefficient (κ) suffers from a relatively large uncertainty in the case of transient chirp dominated lasers since the adiabatic component of the chirp is very small.

Table 3
Extracted parameters from the power and chirp waveform measurements for each DML

Parameter	Units	2.5 Gb/s DML-1	2.5 Gb/s DML-2	10 Gb/s DML
α	–	2.2	5.6	2.7
κ	$\mathrm{Hz\,W^{-1}}$	28.7×10^{12}	1.5×10^{12}	2.0×10^{12}

5.4. Dynamic measurements – IM frequency response measurements

In Fig. 6 the measured small signal IM frequency responses are shown for each DML for

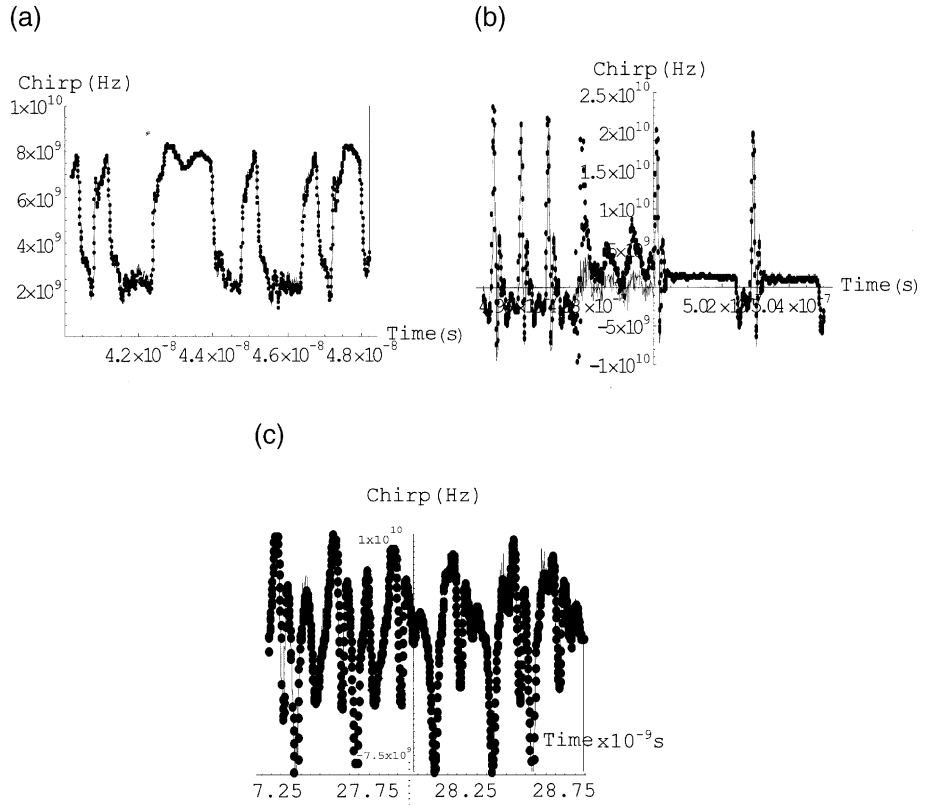

Fig. 5. Measured and fitted chirp waveforms for (a) 2.5 Gb/s DML-1, (b) 2.5 Gb/s DML-2, (c) 10 Gb/s DML.

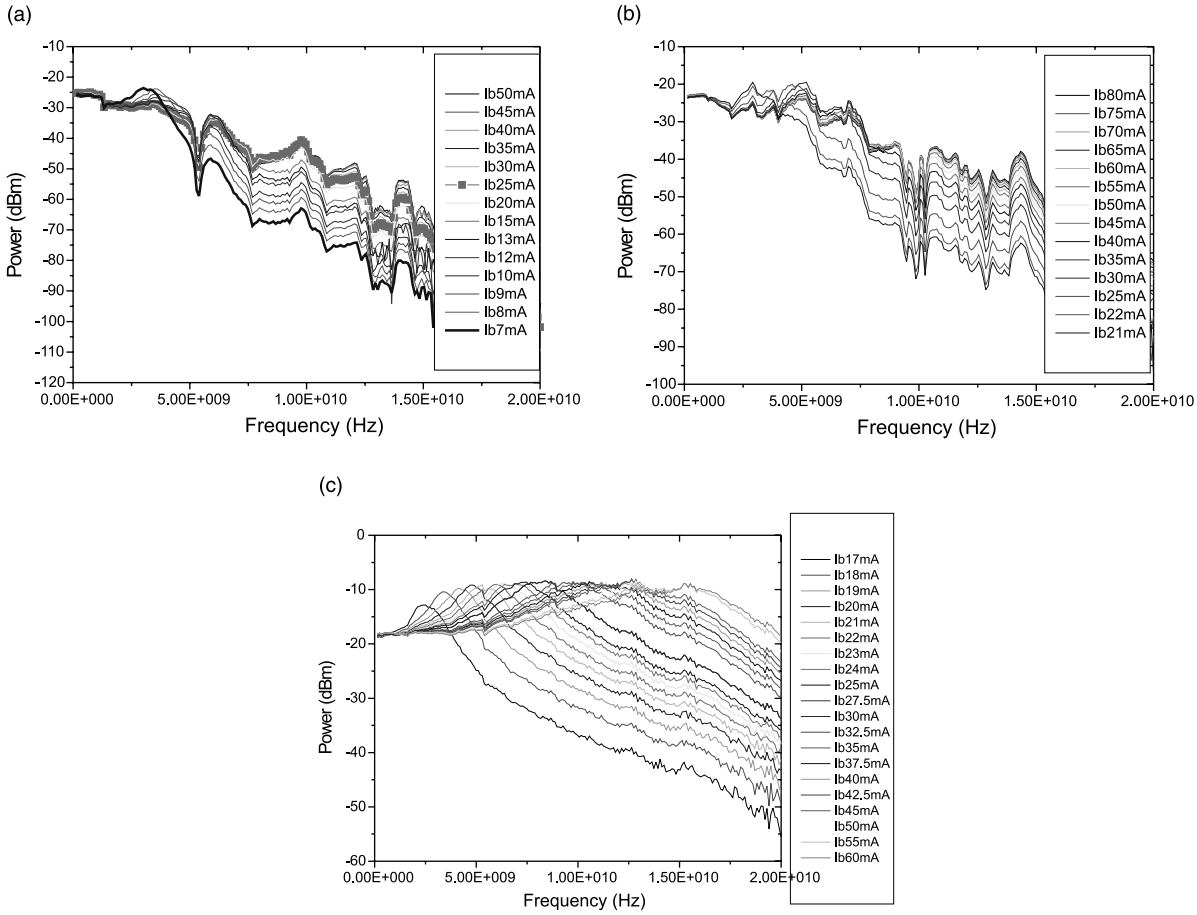

Fig. 6. Measured small signal IM frequency responses for (a) 2.5 Gb/s DML-1, (b) 2.5 Gb/s DML-2, (c) 10 Gb/s DML.

various bias currents. The measured responses include (a) the intrinsic IM frequency response of the DMLs, (b) the parasitics frequency response and (c) any frequency dependence from the equipment used for the measurements. That is the reason why the curves from different DMLs appear to be much different. It is evident from these measurements that the bandwidth is increased for increasing bias currents. At very low bias currents, just above threshold, a resonance peak is evident in the measured responses of all the DMLs. This resonance peak has its origin at the intrinsic laser small signal IM response. In general, for small bias currents it appears to have a small frequency and an intense peak, while the frequency of the peak is shifted to higher frequencies for larger bias currents and the peak is not as pronounced. For larger bias currents it is not so pronounced, because it is filtered out by the parasitic transfer function.

In Fig. 7 the ratios (in dB) of modulation frequency responses corresponding to the various bias currents over the one that corresponds to a bias current just above threshold are plotted. As it has been explained in Section 3.2, these curves are not affected by the laser parasitics neither by any improper calibration of the measuring equipment. The parameters resulted from the fitting of these curves (damping factor and resonance frequency) using Eqs. (20) and (10)–(12) (a fitting example – not the best case is shown in Fig. 8) are plotted in Fig. 9 as a function of the bias currents for each DML. From the slope of the (resonance

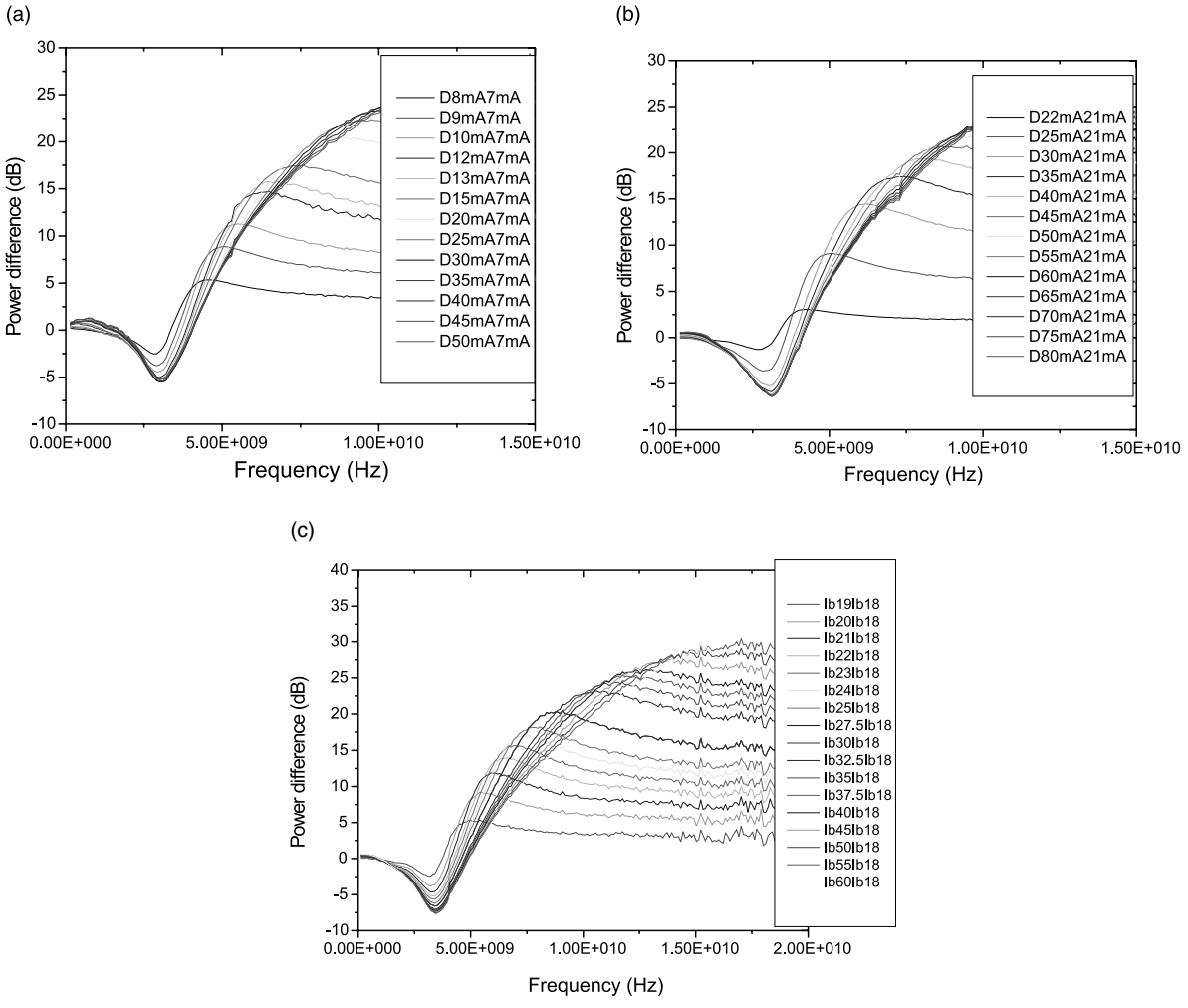

Fig. 7. Ratios (in dB) of modulation frequency responses for (a) 2.5 Gb/s DML-1, (b) 2.5 Gb/s DML-2, (c) 10 Gb/s DML.

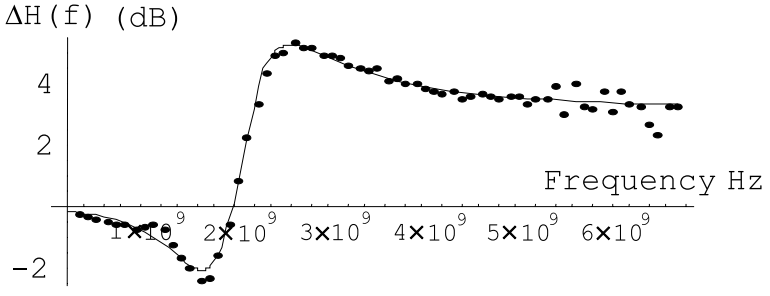

Fig. 8. Fitting example of the ratios (in dB) of the modulation frequency responses.

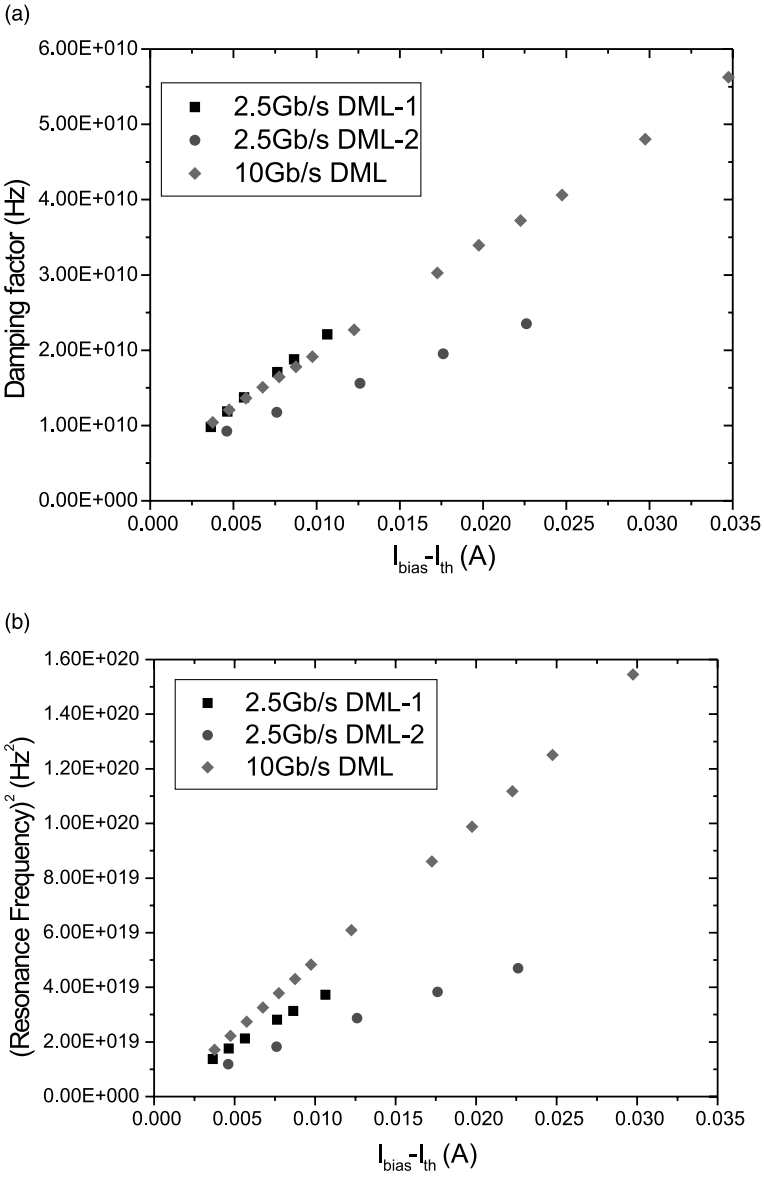

Fig. 9. (a) Damping factor and (b) (resonance frequency)^2 versus the current above threshold for the three DMLs.

Table 4
Extracted parameters from small signal IM frequency response measurements for each DML

Parameter	Units	2.5 Gb/s DML-1	2.5 Gb/s DML-2	10 Gb/s DML
$K = 4\pi^2(\tau_p + \varepsilon/g_0)$	ps	518	420	277
τ_c	ns	0.374	0.256	0.167
$\Gamma g_0/eV$	Hz^2/A	1.848×10^{23}	1.08×10^{23}	2.453×10^{23}

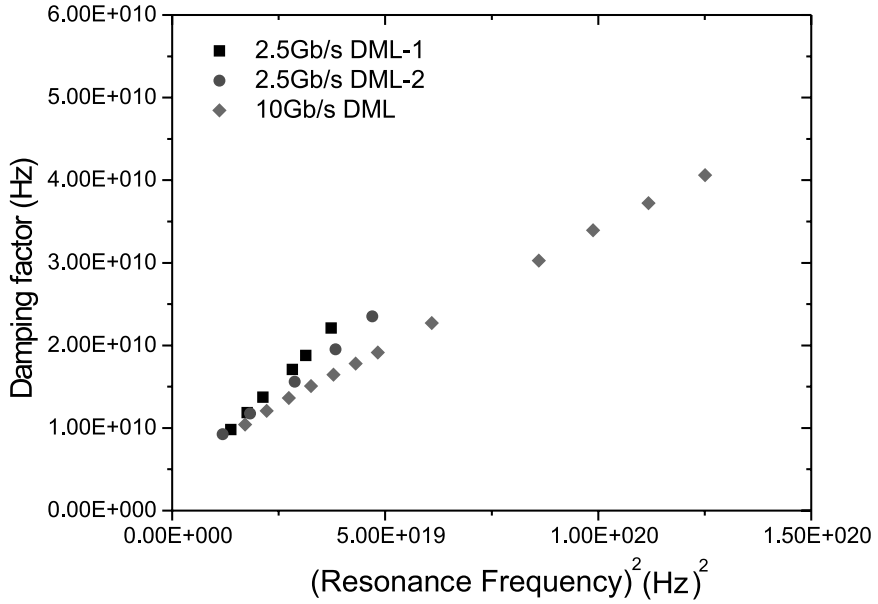

Fig. 10. Damping factor versus the (resonance frequency)^2 for (a) 2.5 Gb/s DML-1, (b) 2.5 Gb/s DML-2, (c) 10 Gb/s DML.

frequency)^2 versus bias current curve we can extract the value of the quantity $\Gamma g_0/eV$. The results are presented in Table 4.

In Fig. 10 the damping factor is plotted versus the (resonance frequency)^2 for each DML. By linear fitting these curves we extract the parameters τ_c, K. The results are also presented in Table 4.

5.5. Parasitic transfer function

From the IM frequency responses, the parasitic transfer function can be determined to some extent. The effects of the device parasitics (including the mount/bond pad) will be present in the IM frequency response. In several studies published in the literature the laser parasitics are assumed to consist of a series resistance and a parallel capacitance. Therefore, the effect of the device parasitics is included as a RC low pass filtering of the modulation current. This filtering will produce a roll-off on the IM response at a frequency that corresponds to the inverse of the RC product. In addition, several studies indicate that carrier-transport effects across the separate confinement heterostructure region in the case of multiple-quantum-well lasers can give a similar roll-off in the frequency response as having a large parasitic capacitance behavior. It is very difficult to experimentally separate the aforementioned effects. Therefore, we take into account both effects by using an effective parasitic transfer function:

$$H_{\mathrm{par}}(f) = \frac{1}{1 + jf/f_c} \tag{21}$$

The overall modulation dynamics are then described by:

$$H_{\mathrm{DML}}(f, I) = H_{\mathrm{par}}(f) + H_{\mathrm{int}}(f, I) \tag{22}$$

where $H_{\mathrm{int}}(f, I)$ is the intrinsic modulation behavior of the laser given be the solution of the rate equations.

In Fig. 11, the measured and calculated small signal IM responses for each 2.5 Gb/s DML are compared. The difference between these curves is imposed by the parasitics. Therefore, a way of extracting the parasitic transfer function is the frequency response subtraction (in dB) of the

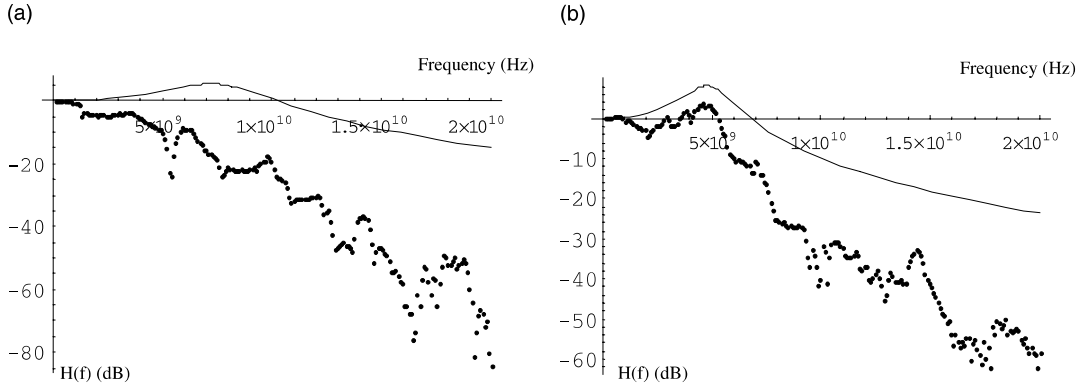

Fig. 11. Comparison of the measured DML IM frequency response (dots) with the intrinsic laser IM response (lines) for (a) 2.5 Gb/s DML-1, and (b) 2.5 Gb/s DML-2.

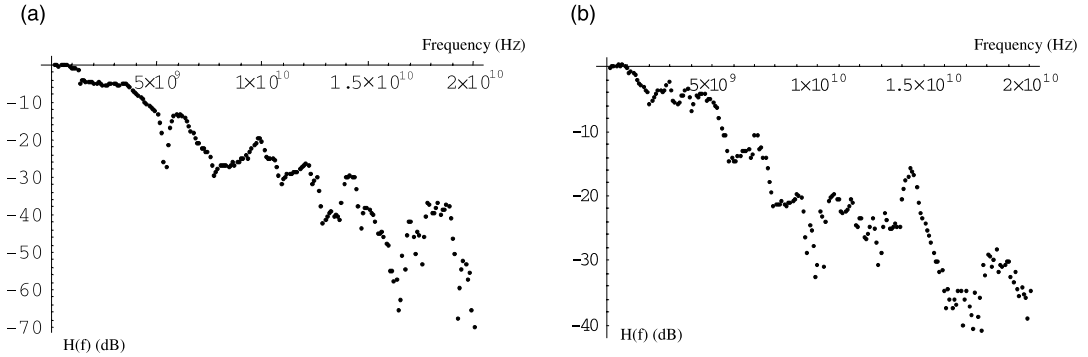

Fig. 12. The extracted parasitic transfer function for (a) 2.5 Gb/s DML-1 and (b) 2.5 Gb/s DML-2.

intrinsic laser small signal IM response from the measured extrinsic one at all bias currents. In general, the parasitic transfer function is not dependent on the bias current. In Fig. 12, the parasitic transfer function for each DML is presented. These curves resulted from the subtraction of the measured DML IM frequency response from the intrinsic laser IM response.

By fitting these curves with Eq. (21) the cut-off frequency can be determined. Obviously the fitting is not good and the modeling of the parasitics will not be ideal but it is a first approximation. Alternatively, the results of Fig. 13 can be used in simulations as is after proper interpolation. The extracted parameters are presented in Table 5. Similar procedure was followed for the 10 Gb/s DML and the results of the extracted cut-off parasitic frequencies for each DML are presented in Table 5.

6. Overall results – comparison of simulated and measured waveforms

In this section we will present comparisons of measured and simulated chirp and power waveforms at the output of the DMLs. In this way, the validity of the rate equations based laser model and the robustness of the parameter extraction procedures will be tested. In the vast majority of previous studies, the validity of the rate equations model was verified mainly by comparison of measured IM power waveforms with the simulated ones. Comparisons of the chirp waveforms are

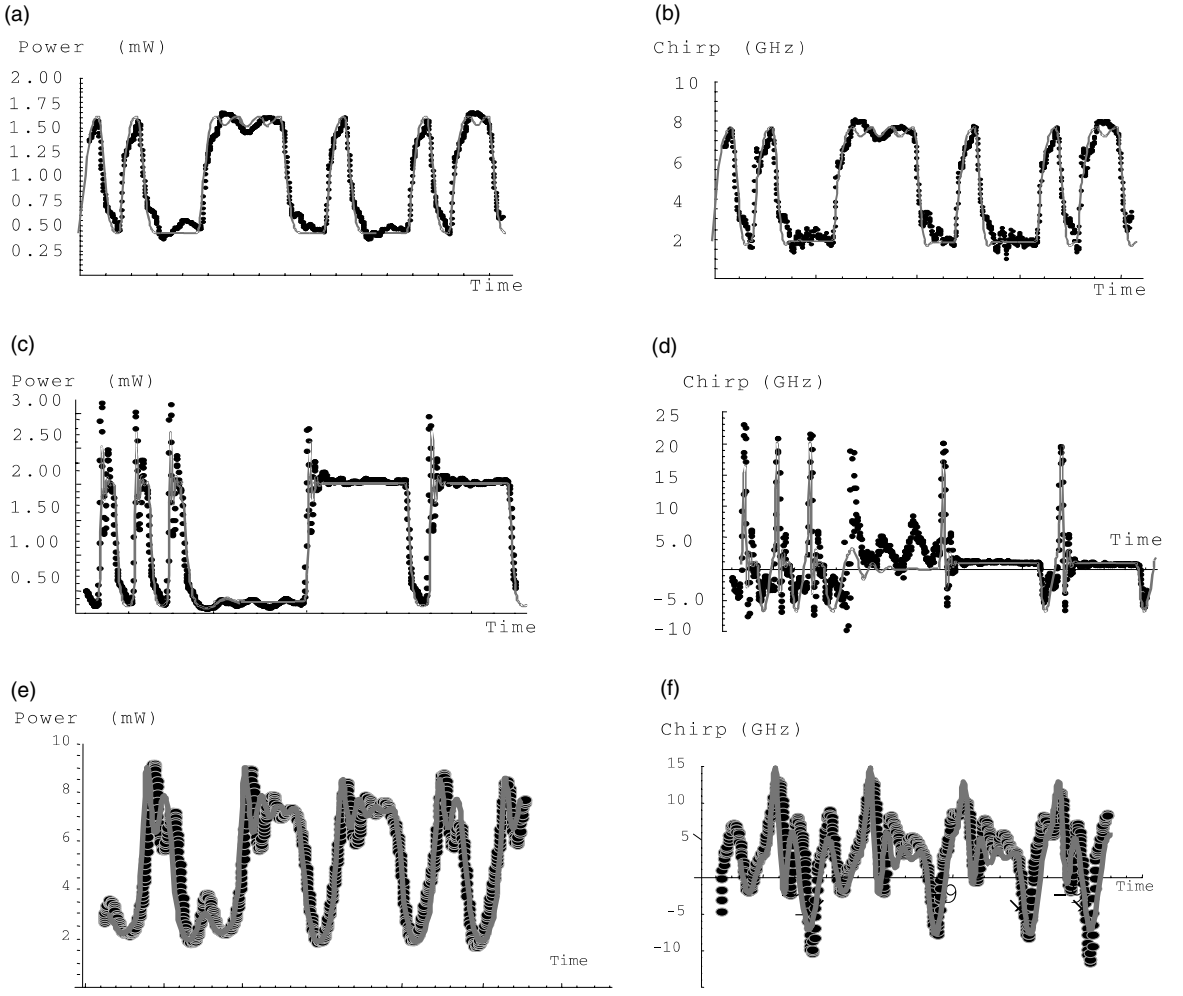

Fig. 13. Measured (dots) and simulated (lines) power (a,c,e) and chirp (b,d,f) waveforms for two different DMLs. Upper row: adiabatic chirp-dominated DML, Bottom row: transient chirp-dominated DML.

Table 5
Extracted cut-off parasitic frequency for each DML

Parameter	Units	2.5 Gb/s DML-1	2.5 Gb/s DML-2	10 Gb/s DML
f_c	GHz	1.48	2.10	9.1

lacking from the literature – with the exemption of Ref. [19] – mainly because of the difficulty of measuring accurately the large signal time-resolved chirp waveforms. However, in this work the demonstration of the validity of the model will be based on comparison of both measured and simulated power and chirp waveforms. In Fig. 13 the measured and simulated power and chirp waveforms for each DML are presented. The simulations have been performed using the rate equations based laser model and the extracted parameters.

The set of laser rate equations has been solved numerically [15]. The simulation conditions were adjusted to the experimental ones. The simulation results for both the power and chirp waveforms and for all DMLs are in strong agreement with the experiment and can predict most of the major

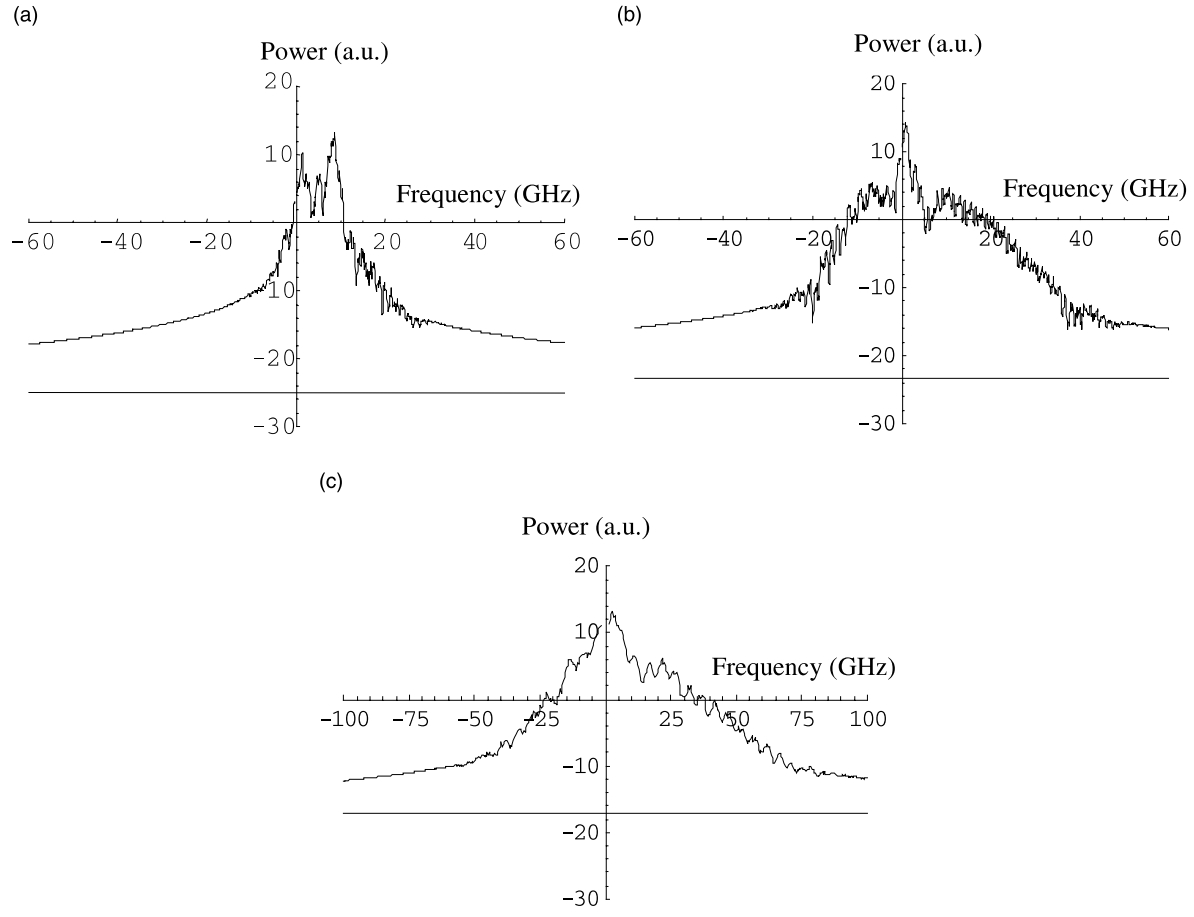

Fig. 14. Calculated optical spectra for (a) 2.5 Gb/s DML-1, (b) 2.5 Gb/s DML-2, (c) 10 Gb/s DML.

features of the measured waveforms (Fig. 13). A more accurate modeling of the laser parasitics will result in even better agreement.

In Fig. 14 the calculated output optical spectra of each DML are shown. The adiabatic behavior of the 2.5 Gb/s DML-1 is apparent. Two distinct peaks are appearing on the spectrum, indicating a strong FM that accompanies the IM under direct modulation [8]. The more intense peak with the higher frequency corresponds to the 1's while the other peak corresponds to the 0's. The transient chirp dominated 2.5 Gb/s DML-2 has optical spectra that are asymmetric with a high frequency bump. Same behavior can be observed for the 10 Gb/s DML, which is also transient chirp dominated.

As it is evident from Fig. 14, different DMLs can experience different shapes of output spectra (depending on whether the DML is transient or adiabatic chirp dominated). The shape of the output spectrum is very crucial when filter concatenation effects in optical networks are considered [30]. Different shapes will interact in a different way with the narrow filter passband in the case of signal passage through a number of MUXs and DMUXs in an optical network and will significantly affect the overall signal quality [30]. As has been discussed in Ref. [30], adiabatic chirp dominated transmitters will result in worst performance in terms of signal degradation due to filter concatenation. Transient chirp dominated DMLs will give small penalties.

7. Use of the modeled DMLs for transmission simulations

Several studies have focused on the theoretical analysis of the impact of the frequency chirp on the system performance [6–8]. However, all the studies have been focused on transmission over fibers with positive dispersion. The decision on the choice of the characteristics of the transmission fiber (i.e. absolute value of dispersion and its sign) for metro applications should first be determined through simulations. Furthermore, no systematic study has been performed for the impact of the chirp characteristics over fibers with either positive or negative dispersion. Having a sufficiently accurate representation of the dynamics of DMLs (Fig. 13), we performed simulations to compare the transmission performance of 2.5 Gb/s DMLs having different chirp characteristics over a distance of 300 km. These simulations utilized two different fiber types that are likely to be used in metro-area networks. Fiber-type-1 is a fiber with the dispersion characteristics of conventional single-mode fiber with positive dispersion of 17 ps/nm/km at 1550 nm (i.e. SMF-28^{TM} fiber). Fiber-type-2 (MetroCor^{TM} fiber) is a novel nonzero dispersion shifted fiber with negative dispersion of about half the absolute dispersion of SMF-28 fiber at 1550 nm [4].

In the case of 2.5 Gb/s simulations, the extinction ratio and the average output optical power at the transmitter was 8.2 dB and 0 dBm respectively. The simulation results (Fig. 15) indicate that the use of negative dispersion fiber resulted in better transmission performance for both adiabatic

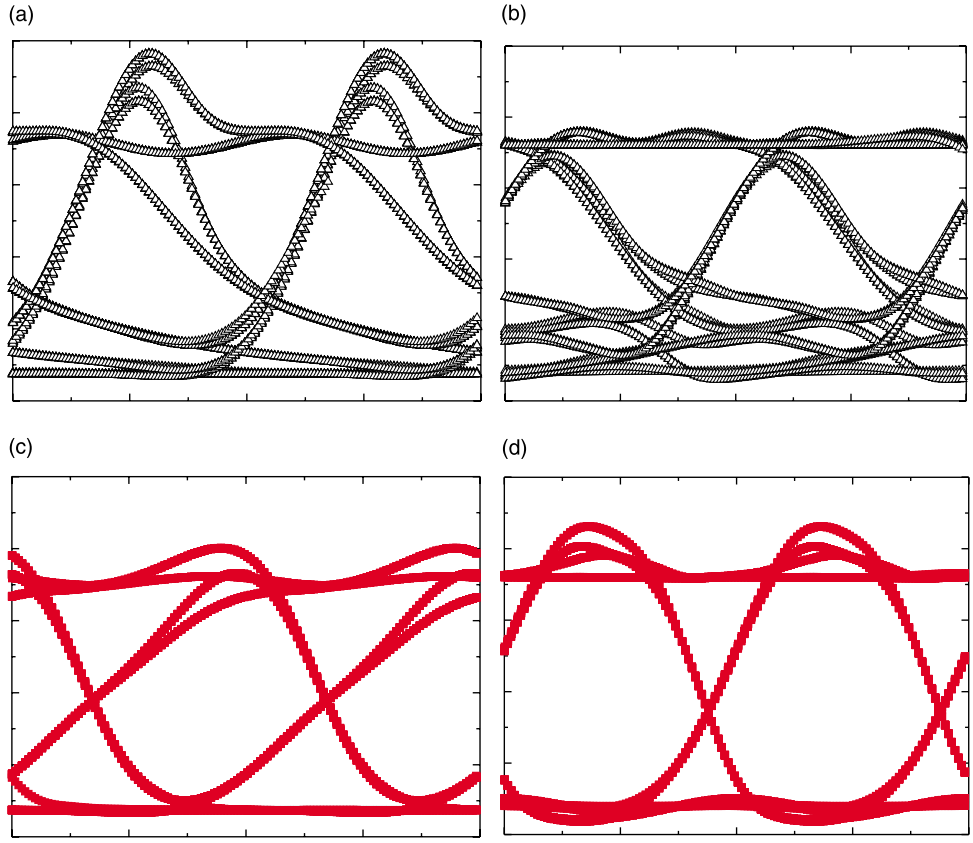

Fig. 15. Received eye patterns after transmission over 300 km for the adiabatic chirp-dominated DML-1 (a,c) and the transient chirp-dominated DML-2 (b,d) over fiber-type-1 (top row) and fiber-type-2 (bottom row).

(Fig. 15(a)) and transient (Fig. 15(b)) chirp dominated DMLs. The eye-diagram after transmission over 300 km of MetroCor fiber is open in both cases of adiabatic (Fig. 15(a)) and transient (Fig. 15(b)) chirp dominated DMLs. A better behavior is observed however for the transient chirp dominated DML. For such DML type, the transmission over SMF-28 results in severe eye closure. Therefore the use of transient chirp dominated DMLs together with use of MetroCor fiber in metropolitan-area networks will result in best overall performance considering both chirp-induced limitations and filter concatenation induced limitations.

Simulations were also performed using the modeled 10 Gb/s DML and the characteristics of MetroCor fiber and it was found that, since the eye-diagram is widely open, transmission over 100 km is possible (Fig. 16). On the contrary, transmission over SMF-28 is limited to less than 20 km. In this case, the extinction ratio and the average output optical power at the transmitter were 5 dB and 6.5 dBm respectively.

The simulation results (Figs. 15 and 16) indicate that a negative dispersion fiber choice will allow for transparent uncompensated metropolitan-area networks over large distances. Conventional fibers will support transparency, but over much shorter distances.

8. Summary

In this paper we present procedures for the extraction of laser rate equation parameters. The measurements were presented in detail. The parameters are extracted using both static and dynamic measurements and fitting procedures. In particular, chirp related parameters are extracted directly through measured chirp and power waveforms. The extracted parameters are used in the large signal single mode rate equation laser model to calculate the power and chirp waveforms. The simulations are compared with the experiments and the agreement is excellent. The procedures have been applied to lasers designed for 2.5 or 10 Gb/s operation. We then applied the rate equation laser model with the extracted parameters to a simulation study that identifies the value of employing a negative dispersion fiber in metro-area networks. It is shown that dispersion shifted fibers with negative dispersion advances the performance of directly modulated lasers used in wavelength division multiplexed metropolitan area transmission systems and networks. At 2.5 Gb/s 300 km transmission is possible with directly modulated lasers and negative dispersion fibers, while at 10 Gb/s an impressive distance of 100 km can be achieved.

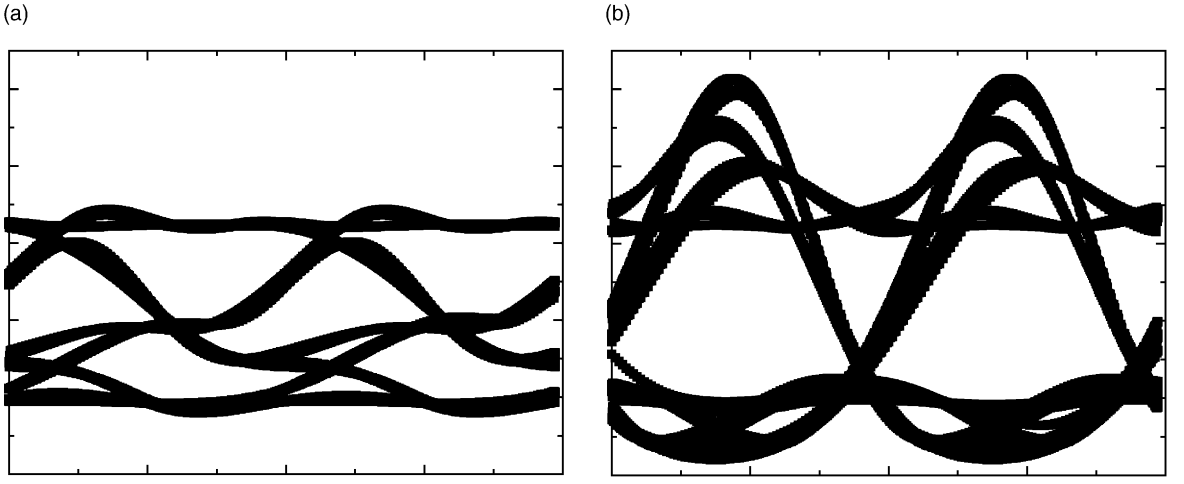

Fig. 16. Received eye patterns for a 10 Gb/s signal after transmission over (a) 20 km of SMF-28 fiber and (b) 100 km of MetroCor fiber.

Acknowledgements

The authors would like to thank the members of the MetroCor fiber team for their helpful comments and suggestions during this work. The first author would like to acknowledge also Dr. Bjerkan and Prof. J. Rosenzweig for useful discussions.

References

[1] G.P. Agrawal, Fiber-Optic Communication Systems, Wiley, New York, 1992.
[2] G. Agrawal, N. Dutta, Long Wavelength Semiconductor Lasers, Van Nostrand Reinhold, 1986.
[3] F. Koyama, Y. Suematsu, Analysis of dynamic spectral width of dynamic-single-mode (DSM) lasers and related transmission bandwidth in single-mode fibers, IEEE J. Quant. Electron. QE-21 (1985) 292–297.
[4] C.-C. Wang, I. Roudas, I. Tomkos, M. Sharma, R.S. Vodhanel, Negative Dispersion fibers for uncompensated Metropolitan networks, ECOC'00.
[5] D. Atlas, A.F. Elrefaie, M.B. Romeiser, D.G. Daut, Chromatic dispersion limitations due to semiconductor lasers chirping in conventional and dispersion-shifted single-mode fiber systems, Opt. Lett. 13 (1988) 1035–1037.
[6] P.J. Corvini, T.L. Koch, Computer simulation of high bit rate optical fiber transmission using single frequency lasers, J. Lightwave Technol. 5 (1987) 1591–1595.
[7] J.C. Cartledge, G.S. Burley, The effect of laser chirping on lightwave system performance, J. Lightwave Technol. 7 (1989) 568–573.
[8] K. Hinton, T. Stephens, Modeling high-speed optical transmission systems, IEEE J. Select. Areas Commun. 11 (1993) 380–392.
[9] R.S. Tucker, High speed modulation of semiconductor lasers, J. Lightwave Technol. 3 (1985) 1180–1192.
[10] S. Kobayashi, Y. Yamamoto, M. Ito, T. Kimura, Direct frequency modulation in AlGaAs semiconductor lasers, IEEE J. Quant. Electron. QE-18 (1982) 582–595.
[11] COST 240 group, Comparison of different DFB laser models within the European COST 240 collaboration, IEE Proc.-Optoelectron. 141 (1994) 82–88.
[12] L.M. Zhang, J.E. Carrol, Large signal dynamic model of the DFB laser, IEEE J. Quant. Electron. QE-28 (1992) 604–611.
[13] S. Hansmann, H. Burkhard, H. Walter, H. Hillmer, A tractable large signal dynamic model – application to strongly coupled distributed feedback lasers, J. Lightwave Technol. 12 (1994) 952–956.
[14] A.J. Lowery, Transmission-line modeling of semiconductor lasers: the transmission-line laser model, Int. J. Numer. Model. 2 (1990) 249–265.
[15] W. Press, B. Flannery, S. Teukolsky, W. Vetterling, Numerical Recipes, Cambridge University Press, Cambridge, 1986.
[16] J. Rosenzweig, private communication.
[17] L. Bjerkan, A. Royset, L. Hafskjaer, D. Myhre, Measurements of laser parameters for simulation of high speed fiber-optic systems, J. Lightwave Technol. 14 (1996) 839–850.
[18] J.C. Cartledge, R.C. Srinisavan, Extraction of DFB laser rate equation parameters for system simulation purposes, J. Lightwave Technol. 15 (1997) 852–860.
[19] K. Czotscher, S. Weisser, A. Leven, J. Rozenzweig, Intensity modulation and chirp of 1.55 μm multiple quantum well laser diodes: modeling and experimental verification, IEEE J. Select. Top. Quant. Electron. 5 (1999) 606–612.
[20] P.A. Morton, T. Tanbun-Ek, R.A. Logan, A.M. Sergent, P.F. Sciortino, D.L. Coblentz, Frequency response subtraction for simple measurements of intrinsic laser dynamic properties, IEEE Photon. Technol. Lett. 4 (1992) 133–136.
[21] J.E. Bowers, High speed semiconductor laser design and performance, Solid State Electron. 30 (1987) 1–11.
[22] P.K. Lau, T. Makino, Effects of laser diode parameters on power penalty in 10 Gb/s optical fiber transmission systems, J. Lightwave Technol. 15 (1997) 1663–1668.
[23] C. Harder, K. Vahala, A. Yariv, Measurement of the linewidth enhancement factor of semiconductor lasers, Appl. Phys. Lett. 42 (1983) 905–907.
[24] T.L. Koch, R.A. Linke, Effect of nonlinear gain reduction on semiconductor laser wavelength chirping, Appl. Phys. Lett. 48 (1986) 613–615.
[25] R.A. Linke, Modulation induced transient chirping in single frequency lasers, IEEE J. Quant. Electron. QE-21 (1985) 593–597.
[26] A. Royset, L. Bjerkan, D. Myhre, L. Hafskjaer, Use of dispersive optical fiber for characterization of chirp in semiconductor lasers, Electron. Lett. 30 (1994) 710–712.
[27] R.A. Saunders, J.P. King, I. Hardcastle, Wideband chirp measurement technique for high bit rate sources, Electron. Lett. 30 (1994) 1336–1337.
[28] ADVANTEST Q7606A/B, Optical chirpform test set, User Guide.
[29] J. Jeong, Y.K. Park, Accurate determination of transient chirp parameter in high speed digital lightwave transmitters, Electron. Lett. 33 (1997) 605–606.
[30] I. Tomkos, R. Hesse, N. Antoniades, A. Boskovic, Impact of filter concatenation effects on the performance of metropolitan area optical networks utilizing directly modulated lasers, Optical Fiber Communications Conference (OFC), 2001.